Shahrood University of Technology

Journal of Mining and Environment (JME)

Journal homepage: www.jme.shahroodut.ac.ir

Iranian Society of Mining Engineering (IRSME)

Investigation of the Effect of Discontinuities on Blast Damage Factor in the Hoek-Brown Failure Criterion for Rock Slope using 3D Discrete Element Modeling

Dariush Kaveh Ahangaran[1], Kaveh Ahangari[1*], and Mosleh Eftekhari[2]

1. Department of Mining Engineering, Science and Research Branch, Islamic Azad University, Tehran, Iran
2. Department of Mining Engineering, Tarbiat Modares University, Tehran, Iran

Article Info

Received 15 May 2024
Received in Revised form 1 August 2024
Accepted 20 August 2024
Published online 20 August 2024

DOI: 10.22044/jme.2024.14532.2735

Keywords

Geological Discontinuities
Geological Strength Index
Peak Particle Velocity
Blast damage factor
3DEC

Abstract

Blast damage on the stability of the slopes plays an important role in the profitability and safety of mines. Determination of this damage is also revealed in the widely used Hoek-Brown failure criterion. Of course, this damage is used as a moderating factor in this failure criterion, and its accurate determination is considered an important challenge in rock engineering. This study aims to investigate the effect of geological structures in blast damage factor using 3D discrete element modeling of two slopes with different directions of geological discontinuities. The dynamic pressure of the explosion is also simulated in three blastholes. To ensure the modeling results, other dynamic properties of the model have been selected based on the proven studies. An analytical analysis was conducted based on the failure zones (blast damage area), and quantitative and qualitative analyses were performed using the recorded PPV values during the blasting simulation. The results show that the geological discontinuities control, damp, and reduce blast damage. The expansion of blast damage is reduced by 75% along with the increase in rock mass strength, and the blast damage can expand up to 33 meters along with the decrease in strength. By reducing the distance of discontinuities, the role of discontinuities in damping becomes greater than other properties of the rock mass and the discontinuities further away from the blasting hole create more damping. The relation between the distance from the Hole and PPV values shows that for more realistic slope stability analysis results, the values of the damage factor in the Hoek-Brown failure criterion should be applied gradually and decreasingly in layers parallel to the slope surface.

1. Introduction

Drilling and blasting is the most economical and widely applied techniques due to its versatility in excavating average to hard rock mass under different geological conditions [1]. During rock blasting, a large amount of energy is released in the form of pressure (up to 50 GPa) and temperature (up to 5000 K) [2]. It is also well known that no more than 30% of energy is spent on breakage and unfortunately, the remainder of the energy is consumed in the form of ground vibrations, back breaks, air blasts, and noise [3]. Under the dynamic pressure of detonation, ground vibration can damage effects on slope stability [2-4].

The damages resulting, based on the geological conditions and the blasting quality, can expand as parallel cracks up to 55 meters away into the mine slopes [5]. Hence, we should consider this damage in the failure criteria to provide more realistic slope stability analysis results [6].

Hoek-Brown (H-B) failure criterion is the most practical failure criterion in rock engineering [7]. This failure criterion was first introduced for the intact rock in 1980. Then, some new editions of the criterion were published in 1988, 1992, and 2002 [8-10]. In the 1988 edition, the “Disturbed” and “Undisturbed” rock mass concepts were introduced to improve the method for wider use in slope

Corresponding author: kaveh.ahangari@gmail.com (K. Ahangari)

stability analysis, reducing the strength properties of the rock masses near the surface and the impact of blast damages [8].

Hoek et al. investigated the relationship between GSI with m_b, a, and s in the 2002 edition, and developed factor D to quantify the blast damage and release stress [11]. They used the "*Blast Damage Factor (D)*" instead of "Disturbed" and "Undisturbed" concepts. To determine factor D, they provided only a table as a simple guide for estimating initial values [12]. In the 2007 edition, Marinos et al. updated the relationships of this failure criterion as the Eqs. (1) to (4); however, still, no more comprehensive guide was provided to determine factor D which has a key role in determining the strength properties of rock mass [13]. The last edition of this failure criterion was provided in 2018; however, the challenge of selecting the factor D value has not been met yet.

$$\sigma_1 = \sigma_3 + \sigma_{ci}(m_b \sigma_3 / \sigma_{ci} + s)^a \quad (1)$$

$$m_b = m_i \exp(GSI - 100 / 28 - 14D) \quad (2)$$

$$s = \exp(GSI - 100 / 9 - 3D) \quad (3)$$

$$a = 1/2 + 1/6(e^{-GSI/15} - e^{-20/3}) \quad (4)$$

Where σ_1 and σ_3 are the major and minor principal stresses at failure; σ_{ci} is the uniaxial compressive strength of the intact rock; a and s are the dimensionless empirical constants; m_i is a curve fitting parameter obtained from triaxle testing of intact rock, and m_b is the reduced value of m_i under rock mass conditions [14].

Eberhardt [10], Zuo and Shen [11] expounded on the details of this failure criterion through comprehensive investigations.

In this investigation, using the 3D discrete element numerical modeling method, the rock mass blasting has been numerically modeled to explain the role of discontinuities in expanding this damage on the rock slope. The slope has been assumed schematically to have two discontinuity modes and five different properties. Blasting modeling was applied as borehole pressure in three blastholes. Using the Fish programming language, the peak particle velocities (PPV) values were monitored along a line from the central blasthole collar to the longitudinal end of the defined model. Then, the spacing of discontinuities decreased to do a greater assessment of the effect of discontinuities. An analytical analysis was conducted based on the probable failure zones, and quantitative and qualitative analyses were performed using the recorded PPV values, and then a table was developed to determine factor D more precisely.

2. Previous investigations on blast damage factor

Sonmez and Ulusay investigated the GIS rock mass classification and found that the main problem with GSI was the lack of a guide to determine the disturbance of rock mass, and finally, they introduced the rock mass disturbance adjustment factor (d_f) to address this problem [15].

Hoek and Karzulovic proposed two factors including stress relaxation and blast damage concerning the application of the H-B failure criterion in surface mines. Thus, they suggested using Sakurai's research to apply the stress relaxation effect. As for the blast damages that can be approximately quantified compared to stress relaxation and explain the reduced rock mass strength comprehensively, a simple method has been proposed based on the blasting method and bench height [6].

Hoek et al. introduced the disturbance factor (D) in the range 0 to 1 and developed a table as a preliminary guide based on the blasting method in response to the subjects outlined by Sonmez and Ulusay (Figure 1) [12].

After introducing the factor D, Sonmez et al. who already emphasized the disturbing impact of mining and blasting on mine slopes investigated factor D and compared it to factor d_f. Finally, they provided a chart to estimate d_f for rock mass disturbance considering the advantages of their factor [16].

Sonmez and Gokceoglu had preliminary discussions with Hoek before the publication of the papers by Hoek and Diederichs [17] and Sonmez et al. [16]. However, they failed to reach an agreement due to the complexities of factor D in estimating rock mass damage. Thus, they proposed a new method to apply the factor d_f in estimating rock mass parameters. In addition, they have developed a simple workflow chart including a guide to using the factor d_f in rock engineering activities [18].

Hoek mentioned the selection of factor D is a technical challenge that appears many times during the use of the H-B failure criterion. In addition, he has mentioned factor D as the "Blast Damage Factor" rather than "disturbance". To end the challenges proposed in the selection of the value and expansion of blast damage, Hoek proposed to

classify the damage between the excavated zone (digging limit) and the undisturbed rock mass for the gradual and decreasing rating of the damage severity from the slope face into the rock mass in a decreasing way. In this regard, numerical modeling recognized a number of layers parallel to the slope face as the factor removing the created challenges [19].

In the last edition of this failure criterion, according to Figure 2, the value of factor D in controlled small-scale blasting was reduced from 0.7 to 0.5. Furthermore, to better estimate the D factor, the method of Rose et al. [20] was declared preferable to using the values presented in Figure 2. However, the determination of the safety factor remains a challenge to rock engineers, and it is a debatable problem considering its effect on the analyses of slope stability and designing optimum slopes of the mine [14].

Appearance of rock mass	Description of rock mass	Suggested value of *D*
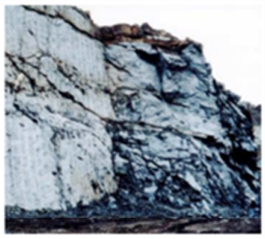	Small scale blasting in civil engineering slopes results in modest rock mass damage, particularly if controlled blasting is used as shown on the left hand side of the photograph. However, stress relief results in some disturbance.	$D = 0.7$ Good blasting $D = 1.0$ Poor blasting
	Very large open pit mine slopes suffer significant disturbance due to heavy production blasting and also due to stress relief from overburden removal. In some softer rocks excavation can be carried out by ripping and dozing and the degree of damage to the slopes is less.	$D = 1.0$ Production blasting $D = 0.7$ Mechanical excavation

Figure 1. Part of the preliminary guide for factor D in slope and based on the blasting method [12]

The disturbance factor *D* should never be applied to the entire rock mass surrounding an excavation		
Appearance of rock mass	Description of rock mass	Suggested value of *D*
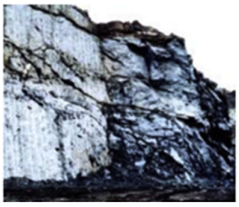	Small-scale blasting in civil engineering slopes results in modest rock mass damage when controlled blasting is used, as shown on the left-hand side of the photograph. Uncontrolled production blasting can result in significant damage to the rock face.	$D = 0.5$ for controlled presplit or smooth wall blasting with $D = 1.0$ for production blasting
	In some weak rock masses, excavation can be carried out by ripping and dozing. Damage to the slopes is due primarily to stress relief. Very large open pit mine slopes suffer significant disturbance due to heavy production blasting and stress relief from overburden removal.	$D = 0.7$ for mechanical excavation effects of stress reduction damage $D = 1.0$ for production blasting A transitional *D* relationship incorporating the effects of stress relaxation can be derived from the disturbance rating[a]

Figure 2. A schematic of the simple updated guide for surface mining by Hoek and Brown [14]

3. Previous modeling of the damage zone

Lu et al. have investigated the rock slope of the Xiluodu Hydropower Station, like what Hoek suggested to determine the blast damage zone. The damage zone is generally defined as the zone beyond the boundary where the rock mass has been considerably damaged or disturbed with values of the damage factor D varying from 1 to 0. To simulate the blast dynamic pressure, a slope

without geological discontinuities was modeled with the 2D finite element method. The modeling results were compared with ultrasonic waves recorded from inside the hole perpendicular to the slope and it was found that the modeling can determine the blast damage zone [21].

Sheng et al. investigated the expansion of blast damage zone in rock slopes with simple geometry (without geological discontinuities) while featuring different slope angles and varying rock properties using the 2D limit equilibrium method, and they developed some charts to analyze the initial stability of slope based on the results [22]. As a complementary study to that of Sheng et al. [22], Qian et al. used two 2D analysis methods to compare the results and to exactly calculate the scope of the blast damage zone [23].

Haghnejad et al. showed that the direction of discontinuities was effective in blast damage expansion through the investigation of a slope in four different discontinuity directions using 3DEC software [24]. In another study, Haghnejad et al. showed that the blast damage factor value in the H-B failure criterion depends on the distance from the blasthole, rock mass properties, and the dip and direction of discontinuities [25].

Chamanzad and Nikkhah worked to investigate the effects of the geomechanical and geometrical parameters of rock and discontinuities on rock mass blasting using the UDEC software. The results obtained show that the discontinuity properties and rock modulus have very significant effects, while the rock density has less of an effect on the rock mass blasting [26].

Afrasiabian et al. investigated the effect of some controllable parameters of blasting using 3DEC software and showed that the distance from the blasthole was the most effective parameter involved in blast damage that would affect the rock mass up to 40 meters [27]. In another investigation by the same researchers, the influence of air-deck was examined using 3DEC software and it was shown that the application of air-deck caused a reduction in blast damage [28].

Ahangaran et al. showed that the blast damage was controlled by geological discontinuities and that it was reduced because of the increase in rock mass strength using 3DEC software [29]. Mousavi et al. proposed a numerical analysis for the nonlinear layering of the blast damage factor value in the H-B failure criterion and the reduction of rock mass strength [30 & 31].

4. Problem statement

Hoek announced that the selection of blast damage factor was a technical challenge in using the H-B failure criterion, and the relevant proposed table was only useful for selecting the initial values. Numerical modeling has been proposed as the course of action used to determine more exact values of the damage factor [19]. The modeling that has been conducted as 2D, includes the limitations of 2D modeling, and they are solely used for initial investigation. The 3D modeling conducted so far has been divided into some categories. Some types of modeling were evaluated solely based on damage to one particular point or simple geometrical instability, while in some other modeling, the borehole pressure was calculated in some others using simple functions. Still, in other types of modeling, the conditions of the rock mass were not complete, and the discontinuities have not been considered in the models.

In some recent 3D investigations, the rock mass damage factor has been studied considering some properties of rock mass, discontinuities, and controllable parameters of blasting. In this study, a schematic slope geometry with two ideal modes of geological discontinuities and a 3DEC numerical modeling was selected to complete the previous investigations. After studying this model, the spacing of discontinuities changed and the result of this change was explored. The details of these examinations have been explained in the following.

4.1. Model geometry

Considering the time-consuming nature of dynamic solutions and also the need for computer hardware, in this model, we examined only 3D numerical modeling of two schematically slopes with three 15-meter benches with a 75° slope thus we could solve different modes and also determine the dynamic effects of the blasting. Therefore, according to the permissible ratio of slope modeling dimensions proposed by Wyllie and Mah [32], the dimensions considered along the X, Y, and Z axes were (0 to 140), (0 to 45), and (0 to 90), respectively.

According to Hustrulid's suggested [33], the blastholes burden was 6.5 m, the spacing was 7.5 m, and the sub-drilling was 3 m. The blast dynamic pressure of ANFO explosive with a density of 780 kg/m^3 and explosion speed of 4052 m/s was applied in three blastholes with a diameter of 200 mm, length of 13 m (10+3), and stemming length of 5 m. All three holes were blasting at the same time and its duration was 0.3 seconds and the total

dynamic pressure was equal to 1040 kg of ANFO explosive. Three discontinuities with a spacing of 10 m have been developed at distances of 13.25, 23.25, and 33.25 m from the blastholes collar at the level of the working bench.

The two models differ only in the direction of the geological discontinuities relative to the slope. In the model of Fig 3-a, the discontinuities have a 45° dip in the opposite direction to the slope face (azimuth 90º), and in Fig 3-b, the discontinuities have the same direction as the slope face (azimuth 270º).

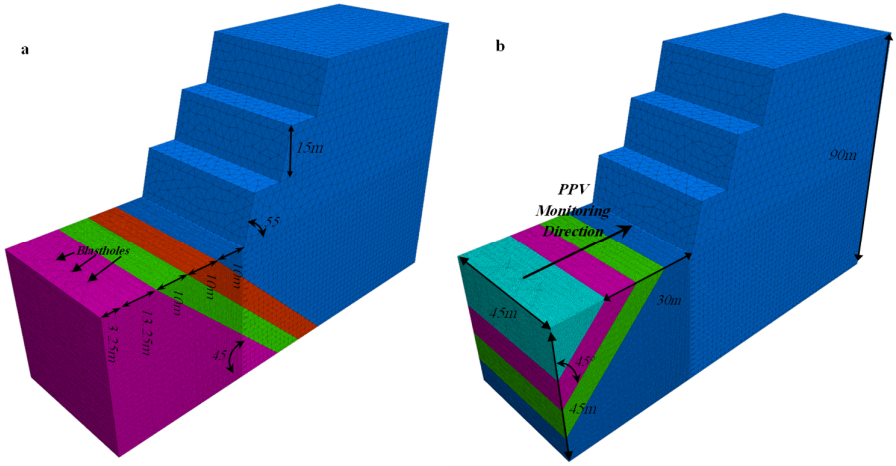

Figure 3 Geometric details of slopes; a) 45° discontinuities in the opposite direction to the slope face and b) 45° discontinuities in the same direction to the slope face.

4.2. Properties of rock mass

According to various research studies such as Rezaei and Seyed-Mousavi [34], the Hoek-Brown failure criterion was chosen to simulate the actual behavior of the rock mass. Hoek and Brown's Indicator index properties for poor, average, and hard rocks [35] are considered intact rock parameters.

The properties of the intact rock and GSI values were used in *RocLab* software to estimate the rock mass properties for three different values (0, 0.7, and 1) of factor D (Table 1). Rocscience *RocLab* is a software program for determining rock mass strength properties, based on the intact rock parameters and the latest version of the generalized Hoek-Brown failure criterion [36]. The reason for choosing these three values of D was to measure the effectiveness of (1) the non-expansion of blast damage, (2) the expansion of controlled blast damage, and (3) the expansion of production blast damage. Estimating the dynamic properties of the rock mass was done similarly to the static state, and its details are mentioned in Table 2. It should be noted that the dynamic values of intact rock properties are estimated from their static values based on the relations proposed by Yilmaz and Unlu [37].

In Tables 1 and 2, the properties with the same GSI values have intact rock properties; however, their rock mass properties vary based on changes in D. Thus, these two values of GSI and D were used in labeling the models. For example, the *GSI75-D0* model represents hard rock properties with GSI and D values of 75 and 0, respectively, according to Figure 3a. The GSI75-D0(1) model has the same properties, but it represents the results related to the geometry of Figure 3b.

Properties of discontinuities were selected based on the classification proposed by Babanouri et al. In this classification, the 30-degree friction angle, 15 kPa cohesion, 0.25 GPa/m shear stiffness, and 0.5 GPa/m stiffness were normal for middle clay filling with a thickness of 10-20 mm [38].

The behavior of the discontinuities was supposed to indicate an elastic-perfectly plastic behavior [25]. The Continuously Yielding Joint Model behavioral model can be also used, but given that the most important discontinuities in the slopes have clay-fillings without roughness, their tensile strength is significantly reduced after the beginning of displacement and is only under the effect of the cohesion force arising from the weight of the upper rock mass, the elastic-perfectly plastic behavior seems more appropriate.

Table 1. Details of static properties of intact rock and rock mass in three classes of poor, average, and hard rocks

Dynamical Properties	*Intact Rock Properties*							Rock Mass Properties									
Simple Litho.	*Den (kg/m³).*	*UCS (MPa)*	*Es (GPa)*	*Poisson*	*mi*	GSI	D	Slope Height (m)	mb	s	a	C (Mpa)	Phi (°)	Sigt (MPa)	Sigcm (MPa)	Erm (GPa)	K (GPa)	G (GPa)
Granites	2700	150	64	0.20	25.0	75.0	0.0	100	10.24	6.2E-02	0.50	4.1	63	-0.91	69	52	29	22
Granites	2700	150	64	0.20	25.0	75.0	0.7	100	6.33	2.7E-02	0.50	3.0	61	-0.63	53	26	15	11
Granites	2700	150	64	0.20	25.0	75.0	1.0	100	4.19	1.6E-02	0.50	2.5	58	-0.55	43	17	10	7
Sandstone	2500	80	22	0.25	15.0	50.0	0.0	100	2.52	3.9E-03	0.51	1.1	52	-0.12	17	7	5	3
Sandstone	2500	80	22	0.25	15.0	50.0	0.7	100	0.96	7.1E-04	0.51	0.7	45	-0.06	10	2	2	1
Sandstone	2750	80	22	0.25	15.0	50.0	1.0	100	0.42	2.4E-04	0.51	0.5	38	-0.05	7	1	1	1
Breccia	2300	20	10	0.30	8.0	30.0	0.0	100	0.66	4.2E-04	0.52	0.3	31	-0.01	2	1	1	0
Breccia	2300	20	10	0.30	8.0	30.0	0.7	100	0.17	3.9E-05	0.52	0.2	21	0.00	1	0	0	0
Breccia	2300	20	10	0.30	8.0	30.0	1.0	100	0.05	8.6E-06	0.52	0.1	14	0.00	1	0	0	0

Table 2. Details of dynamic properties of intact rock and rock mass

Dynamical Properties	*Intact Rock Properties*							Rock Mass Properties									
Simple Litho.	*Den (kg/m³).*	*UCS (MPa)*	*Es (GPa)*	*Poisson*	*mi*	GSI	D	Slope Height (m)	mb	s	a	C (Mpa)	Phi (°)	Sigt (MPa)	Sigcm (MPa)	Erm (GPa)	K (GPa)	G (GPa)
Granites	2700	278	100	0.20	25.0	75.0	0.0	100	10.24	6.2E-02	0.50	6.9	66	-1.69	128	82	45	34
Granites	2700	278	100	0.20	25.0	75.0	0.7	100	6.33	2.7E-02	0.50	4.9	64	-1.17	99	41	23	17
Granites	2700	278	100	0.20	25.0	75.0	1.0	100	4.19	1.6E-02	0.50	4.1	61	-1.03	80	27	15	11
Sandstone	2500	149	35	0.25	15.0	50.0	0.0	100	2.52	3.9E-03	0.51	1.5	56	-0.229	32	11	7	4
Sandstone	2500	149	35	0.25	15.0	50.0	0.7	100	0.96	7.1E-04	0.51	1.0	49	-0.110	19	4	3	2
Sandstone	2750	149	35	0.25	15.0	50.0	1.0	100	0.42	2.4E-04	0.51	0.7	43	-0.085	13	2	2	1
Breccia	2300	37	16	0.30	8.0	30.0	0.0	100	0.66	4.2E-04	0.52	0.4	36	-0.02	4	1	1	1
Breccia	2300	37	16	0.30	8.0	30.0	0.7	100	0.17	3.9E-05	0.52	0.2	25	-0.01	2	1	0	0
Breccia	2300	37	16	0.30	8.0	30.0	1.0	100	0.05	8.6E-06	0.52	0.1	17	-0.01	1	0	0	0

4.3. Static solution

According to the studies by Wei-hua et al. [39], and Azizabadi et al. [2], the mesh dimension of the model was considered as one-tenth of the smallest wavelength i.e. equal to two. After creating the geometries, the models were solved statically based on the properties of Table 1 to reach the initial equilibrium state. However, the models reached the initial equilibrium state only in five strengthen models while weaken models including *GSI50-D1*, *GSI30-D0*, *GSI30-D0.7*, and *GSI30-D1* models did not achieve the initial equilibrium state, and their geometry collapsed.

4.4. Simulation of borehole pressure

Equations of mode and simple pressure functions have disadvantages according to the results of Yilmaz and Unlu [39], and they have suggested the use of a pressure decay function to simulate borehole pressure.

The results of Mckenzie's [40] investigation, which showed the borehole pressure caused by ANFO explosion in a hole with a diameter of 200 mm and a length of 15 m, equal to 2.6 GPa, was used to verify the accuracy of the pressure simulation. The pressure decay function of Jong et al. [41] calculated the maximum dynamic pressure to be 1.6 GPa. The values estimated by Yang et al. [1] functions were also different from Mckenzie's value. Finally, based on Aliabadian and Sharafisafa's [42] Eqs. (5) to (9) and the functions they used, the maximum borehole pressure was estimated at 2.5 GPa. This function uses the density, bulk modulus, shear modulus, and rock P-wave velocity parameters of rock for estimation, which makes the pressure decay function dependent on the condition of the rock. Therefore, its functions were used to simulate borehole pressure (in the form of a pressure wave).

$$PD = 432\times10^{-6}\frac{\rho_e V_d^2}{1+0.8\rho_e} \quad (5)$$

Where PD is blast pressure (MPa), ρ_e explosive density (gr/cm^3), and V_d detonation velocity (m/s). Gas pressure (PE) usually is considered half of the blast pressure, e.g.:

$$PE = \frac{1}{2}PD \quad (6)$$

$$PW = PE(\frac{r_h}{r_e})^{-qk} \quad (7)$$

Where r_h is the blasthole diameter (mm), r_e diameter of an explosive charge (mm), q specific

heat coefficient, and k shape factor of explosive (3 for cylindrical charges).

$$P(t) = PW \frac{8\rho_r C_p}{\rho_r C_p + V_d \rho_e}\left[e^{(-Bt/\sqrt{2})} - e^{(-\sqrt{2}Bt)}\right] \quad (8)$$

$$B = 16338$$

$$C_p = \sqrt{(K + 4G/3)/\rho} \quad (9)$$

Where ρ_r is the rock mass density (gr/cm^3), C_p P-wave velocity (m/s), t time (s), K and G are bulk modulus and shear modulus (Pa). Based on the different properties of the rock, five different borehole pressures were simulated for the models. Figure 4 shows the changes in profile histories in these five borehole pressures for the ANFO explosive.

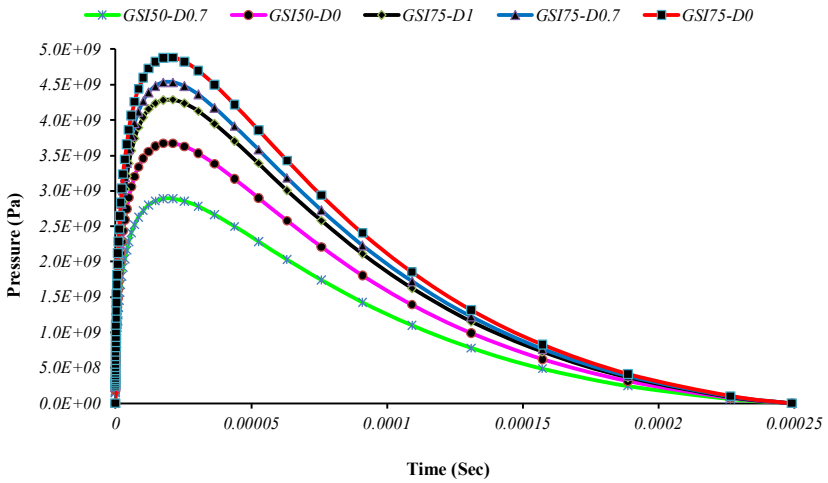

Figure 4. Pressure–time profile histories applied on the blastholes' wall for the ANFO explosive

One of the most influential factors in reliable blasting simulation is determining its mechanism. The mechanisms of Gas Pressurization, Stress Wave, and Reflection of Stress Wave [43] mainly exist in the blasting, which is used in this study as follows:

- ✓ To create conditions for Gas Pressurization, the meshing of the model along the burden, the entire model width, and blasthole height have the possibility of expansion in the X axis (in the direction of the free surface face).
- ✓ Resende [44] has proposed three methods to apply dynamic pressure (Figure 5). According to the recorded results of some researchers that the diameter of the hole is effective in the weight of the explosive and also in the blast pressure, the blast dynamic pressure was loaded in the form of stress wave throughout the blasthole.
- ✓ It was possible to reflect stress waves in all three axes into the rock mass using 3DEC capabilities and relaxation of boundaries on the free surface (without viscous boundaries).

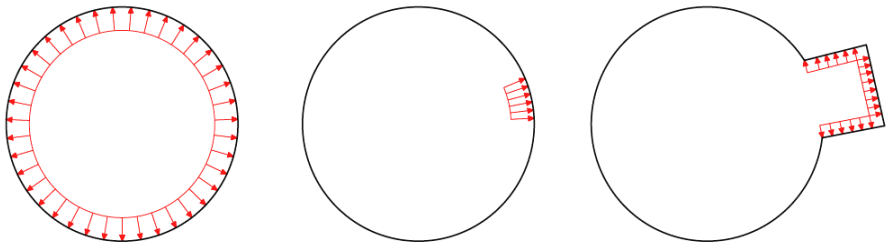

Figure 5. Three methods of applying blast pressure: loading throughout the blasthole (left), loading in an element face (center), and loading in a removed element (right) [41]

4.5. Damage estimation parameters

Based on the suggestions of Drukovanyi et al. [45] and Liu [46], the applied pressure or stress due to compatibility with the mechanical behavior of the rock was chosen as the first critical parameter characterizing the damage. Also, based on the suggestion of Hustrulid et al. [47] and Persson et al. [48], PPV due to the ease of measurement was used as the second critical parameter.

The applied pressure or stress has been used to determine possible failure zones in 3DEC software and qualitatively in damage assessment. PPV has also been used quantitatively to assess damage. Based on the suggestion of Bhandari to reduce the risk of damage, the value of 50 mm/s was chosen as the safe vibration threshold [49].

Using the FISH programming language, coding was done for monitoring and recording PPV values. Then the scene codes were loaded into 3DEC to record the values in a longitudinal direction from the central blasthole collar to the end of the model. In other words, the PPV monitoring axis was defined at X=0 to 140, Y=22.5, and Z=45 m to make it possible to record the vibration generated at the bench surface of the model.

4.6. Dynamic simulation

To prevent the reflection of stress waves into the model, based on the proposal of Yilmaz and Unlu [36], the dynamic boundaries of the model were defined as viscous on the sides (except for the free surface) and at the bottom. Based on the suggestion of the same researchers, the damping of the model was also considered as a local damping of 5%. Also, due to the not-so-importance of Rayleigh damping in materials with plasticity behavior, its use was omitted. The dynamic simulation started by applying borehole pressures on blasthole walls according to any given model. According to the expanded Fish, the PPV values caused by blast dynamic pressure were recorded during the simulation.

5. Results and discussion

5.1. Probable failure zones of standard models

Plastic indicators of failure in 3DEC based on the increase in the plastic flow of stresses on the zones provide the probable yield criterion in the form of various state patterns [50]. Using this feature, probable failure zones of the standard model with different geologic discontinuity directions relative to the slope face are displayed against each other in Figs 6 and 7 so that the role of discontinuities in controlling the expansion of different types of shear and tensile failures towards the slope can be compared. The *p* and *n* index in each of the failures represent the *past* and *now* failures, respectively.

As shown in Figure 6a, the *Shear-p* failure due to the initial blast dynamic pressure has expanded progressively from the beginning to the end of the model and then ended. The *Shear-p Tension-p* failures showed the second shear-tensile failure developed in the model that continued and ended after the initial shear failure (*Shear-p*). *Shear-n Shear-p Tension-p* failures have mostly expanded further away from the burden. This failure starts as tensile and converts into the shear failure where still a new shear failure develops 0.3 seconds after the blasting. Probably multiple repetitions of (1) transfer of waves to the free surface, (2) reflection of waves to the rock mass and (3) re-transferring to the free surface due to new fragmentation processes are the main reasons for these complicated failures. Another complicated failure exists accordingly further from the rock burden that expands as *Shear-n Tension-n Shear-p Tension-p* which complements the previous failure. Tensile failures follow the theory for converting stress waves to tensile waves because of the reflection of the waves at the free surface [3], and the shear failures are directly created by the dynamic pressure caused by blasting. Other pressures pointed out in the figure guide have developed in very limited zones that are not very important.

As shown in Figure 6b, the effects of discontinuities become more apparent by changing the direction of discontinuities. The first discontinuity has managed to control well *Shear-n Shear-p Tension-p* and *Shear-n Tension-n Shear-p Tension-p* and the second discontinuity also has controlled the *Shear-n shear-p* failure. What both Figures 6a and b have in common is that they both follow the expansion of plastic flow from the discontinuities.

The second and third discontinuities in Figure 6c control the shear failure more clearly compared to the *GSI50-D0.7* model where the difference between their rock mass properties from different values of D. The surface progression of *Shear-p* on benches has decreased, and the *Shear-p Shear-p* failure features less deep expansion. Of course, it is considered to be the main failure in the burden. The comparison between these two models shows that the first and second discontinuities have controlled the *Shear-p* failure more effectively.

Comparing the progression of the failures in Figure 6d with that of Figure 6b model shows that the development of *Shear-p Shear-p Tension-p* failure has decreased along with the increase in the rock mass strength (due to the reduction in D). In addition, the changes in *Shear-n Shear-p Tension-p* and *Shear-n Tension-n Shear-p Tension-p* failure have also decreased. These two failures are still expanding around the blasthole relative to the *GSI50-D0* model. The discontinuity direction and

the reflection of waves from their surface can create these two failures. Probably, a greater fragmentation will occur in these two failures in the rock mass. In general, the failures have decreased both quantitatively and qualitatively along with the increase in rock mass strength due to a decrease in D, and rock mass disturbance resulting from the dynamic pressure of the blasting has decreased.

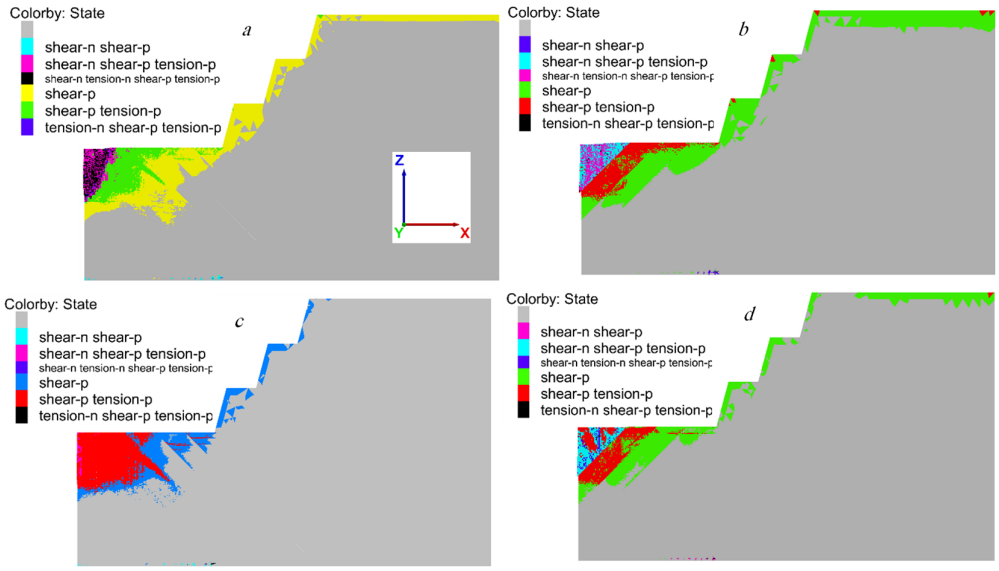

Figure 6. Rock mass failure condition 0.3 seconds after the blasting in standard models: a) *GSI50-D0.7*; b) *GSI50-D0.7(1)*; c) *GSI50-D0*; and d) *GSI50-D0(1)*

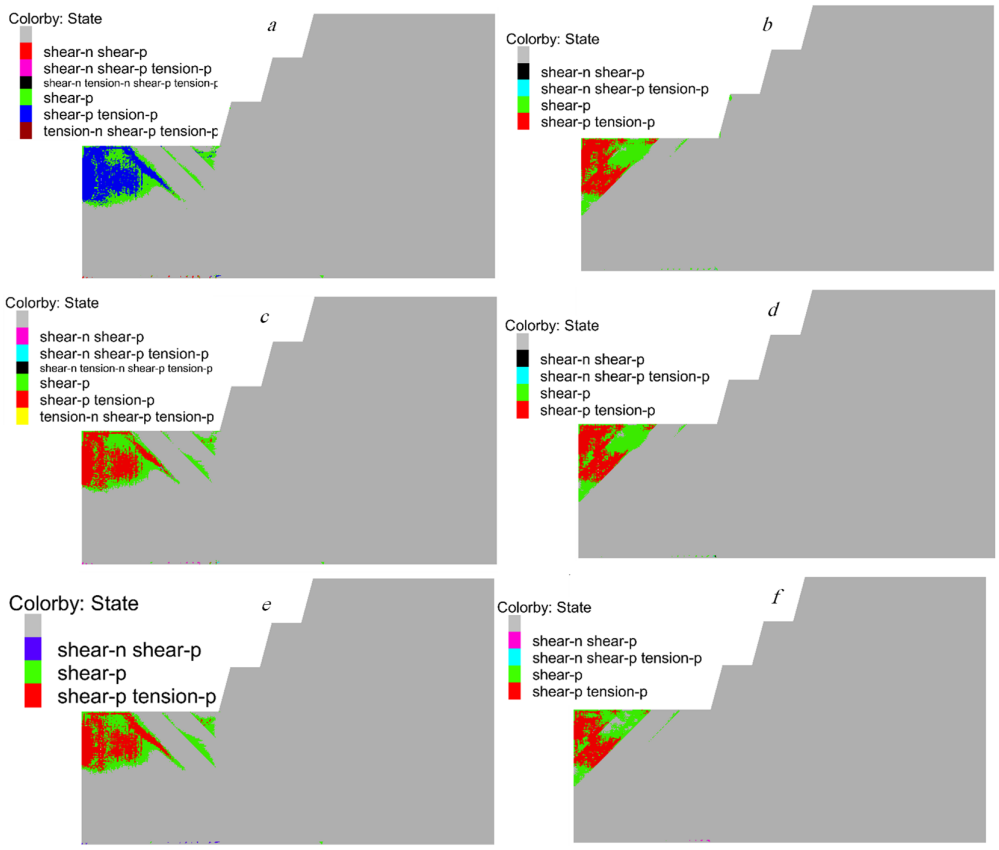

Figure 7. Failure zones in 0.3 s after the blasting in standard models: a) *GSI75-D1*; b) *GSI75-D1(1)*; c) *GSI75-D0.7*; d) *GSI75-D0.7(1)*; e) *GSI75-D0;* and f) *GSI75-D0(1)*

The failures in Figure 7a have decreased along with the increase in rock mass strength relative to previous models both qualitatively and quantitatively. Qualitatively, only two failures of *Shear-p* and *Tension-p Shear-p* are more important. Quantitatively, the *Shear-p* failure could only pass through the first discontinuity.

The quantitative and qualitative reductions in failures are tangible in Figure 7b similar to that of the *GSI75-D1* model compared to failures with weaker rock mass (Figures 6a-d). However, less *Shear-p* failure has passed through the first discontinuity compared to the *GSI75-D1* model.

The same quantitative and qualitative reduction ratio in failures is evident in Figures 7c and d along with the increase in rock mass strength. The same trend is shown in Figures 7e and f. The direction of discontinuities having the same as the slope face has managed to control the dynamic pressure of blasting more effectively, and the toe of the slope has undergone less plasticity and disturbance.

5.2. Recorded PPVs of standard models

Along the monitoring axis, the recorded PPVs of models according to Figure 3a have been shown in Figures 8 and 9 and then recorded PPVs of models according to Figure 3b, have been presented in Figure 10. In Figure 8, each discontinuity has reduced dynamic blast pressure, and then their PPV value has decreased evidently.

According to Figure 9a, by decreasing factor D and consequently increasing the rock mass strength, the recorded PPV values generally decreased compared to those in Figure 8. In addition, the reduction in PPV value becomes more evident after each discontinuity. The changes in PPV value in burden also depend on the multiple repetitions of reflection of shear waves to the free surface and its tensile re-transferring within the rock mass that was formerly observed as the failure of *Shear-n Shear-p Tension-p* and *Shear-n Tension-n Shear-p Tension-p*. Figures 9b and c again show the reduction in PPV value along with the increase in rock strength, and reduction in this value after each discontinuity. This shows that the rock mass strength increases along with the increase in GSI or D values while the blast damage decreases. This can be used to study the stability of slopes and blast design in hard and average rock mass.

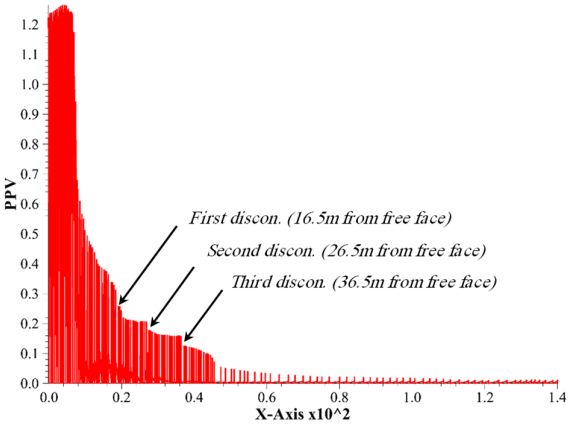

Figure 8. PPV (m/s) values recorded in *GSI50-D0.7* model and monitoring axis direction X=0-140 m, Y =22.5 m, and Z= 45 m

According to Figure 10a, the PPV value at the free surface was greater than that of Figure 8. According to Figures 6 and 7, the same direction of first discontinuity reflects most waves to the free surface; thus, there will be more and greater failures in burden. When the opposite direction of the discontinuities transfers these waves into the rock mass, in contrast to Figures 8 and 9 in which PPV values decreased almost in the same stages amongst the discontinuities, the PPV value in Figure 10a increased before each discontinuity and decreased suddenly after it. This occurs because in this case, the discontinuities reflect dynamic blast waves. The items mentioned in Figure 10a can be also observed in Figures 10b to e.

The comparison between the decrease in PPV value to the increase in distance from the blasthole shows some changes that are not consistent with the charts obtained from the empirical models of PPV prediction (Figure 11). The empirical models are often developed based on statistical methods [51]. The main reason for this inconsistency is the exclusion of geological discontinuities [52]. This is the case because these models are formed through the general form of Eq. (10), where b is the blast design coefficient and k is the geological coefficient. Coefficient k is unable to transfer the influence of geological discontinuities in these models [25]. Parameter D in these models is the distance from the blasthole.

$$PPV = kD^{-b} \quad (10)$$

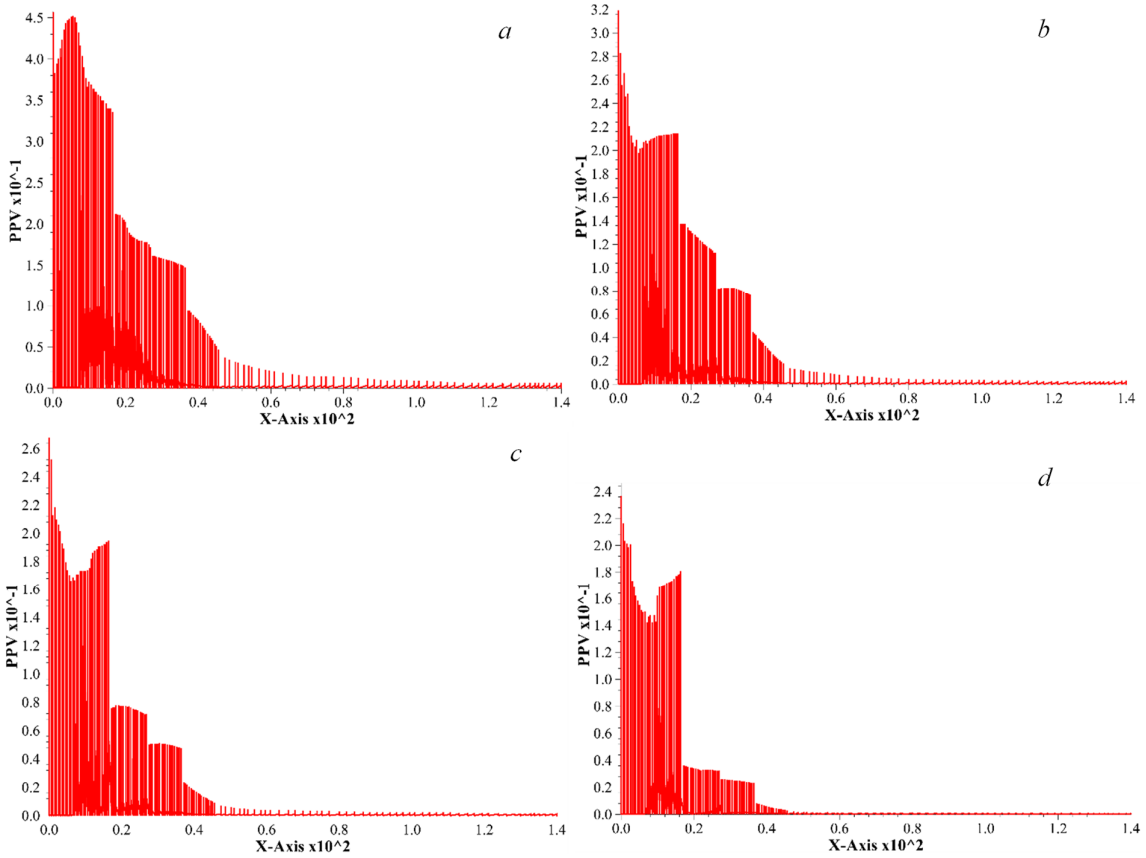

Figure 9. PPV (m/s) values recorded in the first mode of standard models: a) *GSI50-D0*; b) *GSI75-D1*; c) *GSI75-D0.7*; and d) *GSI75-D0*

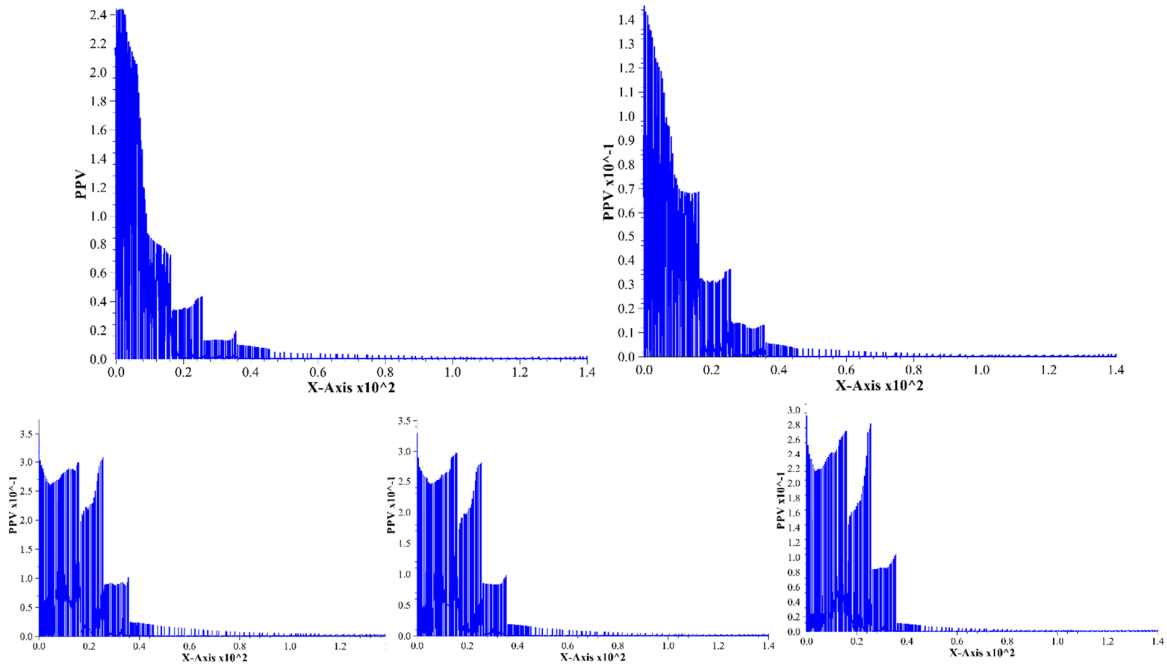

Figure 10. PPV values recorded in the second mode of standard models: a) *GSI50-D0.7(1)*; b) *GSI50-D0(1)*; c) *GSI75-D1(1)*; d) *GSI75-D0.7(1)*; and e) *GSI75-D0(1)*

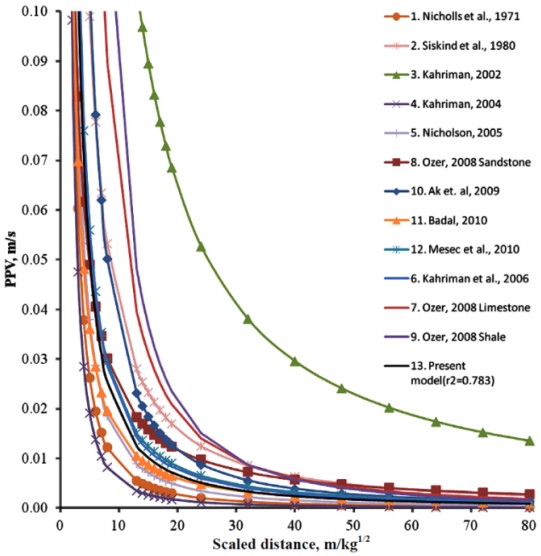

Figure 11. Summary of empirical PPV predicting model [52]

5.3. Effect assessment of discontinuity spacing

The rock mass with discontinuities has different spacing. Thus, in this investigation, the spacing of discontinuities decreased from 10 to 5 m to determine its effect. The placement of the third discontinuity accords with the standard model and this decrease in the distance was created by the displacement in two other discontinuities. The first, second, and third discontinuities are at distances of 23.25, 28.25, and 33.25 meters from the blasthole collar. Figures 12 and 13, respectively, show the models in Figures 3a and b.

Here, the main observable difference from the standard models is the sudden increase in PPV value in the first discontinuity. This is the case because, on the one hand, a large part of blast waves collides with this discontinuity and thus are reflected; on the other hand, the waves passing through it collide with the second and third discontinuities, and some of them are reflected towards the first discontinuity. Considering the decrease in the spacing of discontinuities, the level of rock mass damping between the discontinuities also decreased, and the waves reflected from the second discontinuities still have enough energy to affect the value of the first discontinuity and increase the PPV value.

In these models, PPV value decreases in general along with the increase in GSI and D values, and the trend of changes in PPV values are similar to each other in both modes of discontinuity direction. The discontinuities have an effective role in the PPV values and thus in the rock mass damage both quantitatively and qualitatively. The main difference between Figures 12 and 13 is the increase in PPV in the discontinuities with the same direction of the slope.

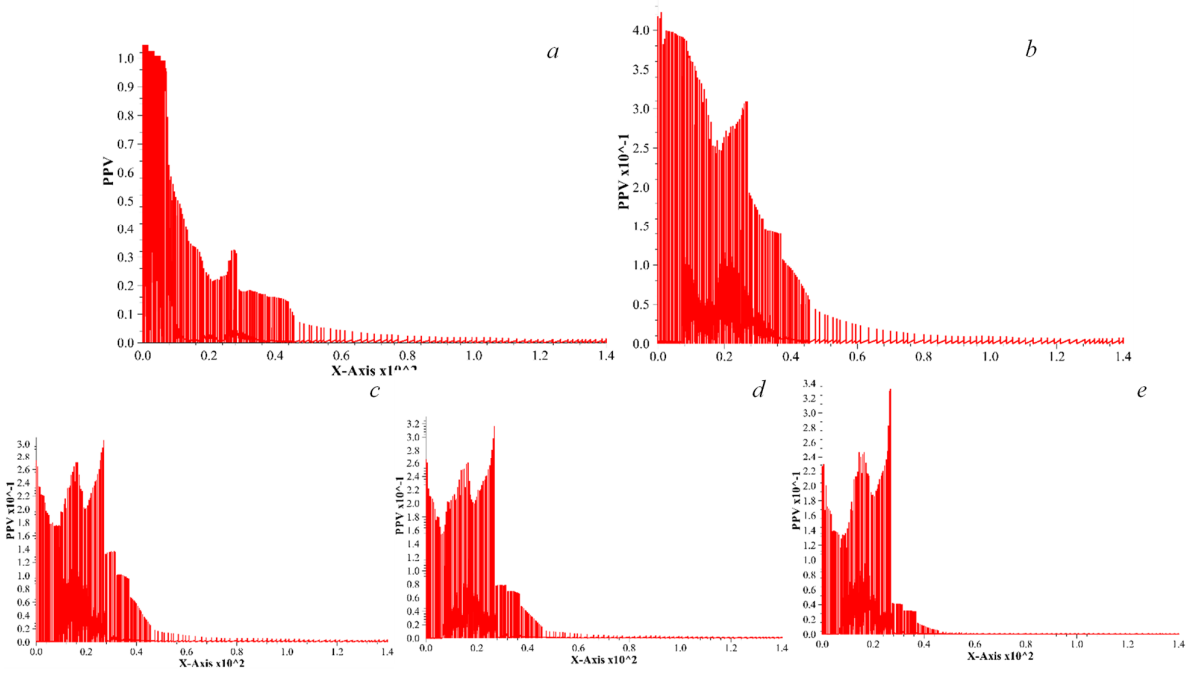

Figure 12. PPV values recorded in assessing the effect of discontinuities spacing in models: a) GSI50-D0.7; b) GSI50-D0; c) GSI75-D1; d) GSI75- D0.7; and e) GSI75-D0

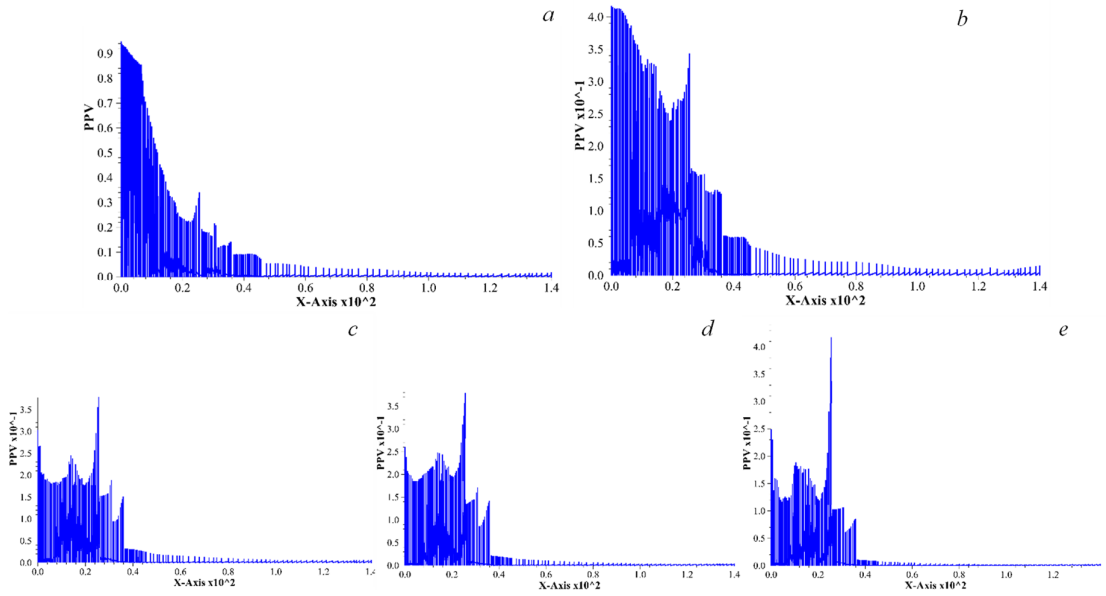

Figure 13. PPV values recorded in assessing the effect of discontinuities spacing in models: a) *GSI50-D0.7(1)*; b) *GSI50-D0(1)*; c *GSI75-D1(1)*; d) *GSI75-D0.7(1)*; and e) *GSI75-D0(1)*

5.4. Statistical analysis of standard model

To study the role of discontinuities quantitatively, the greatest PPV value on discontinuity surfaces was selected at the distances of 13.25, 23.25, and 33.25 m from the blasthole collar were selected, and they were provided with similar values at blasthole collar for both modes of discontinuities in Tables 3 and 4. This selection was made to determine the expansion of blast damage considering the properties of the rock mass of each model. The values greater than ***50 mm/s*** indicated rock mass damage that has been shown in **Bold** and *Italic* styles.

Table 3. The greatest PPV values above the blasthole collar and discontinuities surface in the first mode of discontinuities according to Figure 3a

Location (m) from Blastholes	PPV Max (mm/s)				
	GSI50-D0.7	GSI50-D0	GSI75-D1	GSI75-D0.7	GSI75-D0
0	1263.7	449.6	201.8	168.4	150.4
13.25	355.3	212.3	135.6	74.9	33.6
23.25	167.5	159.3	79.7	47.3	24.2
33.25	113.7	91.7	42.2	21.2	7.1

Table 4 Greatest PPV values above the blasthole collar and discontinuities surface in the second mode of discontinuities according to Figure 3b

Location (m) from Blastholes	PPV Max (mm/s)				
	GSI50-D0.7 (1)	GSI50-D0 (1)	GSI75-D1 (1)	GSI75-D0.7 (1)	GSI75-D0 (1)
0	1859.4	982.1	263.5	244.0	221.9
13.25	315.2	310.5	197.8	170.2	142.3
23.25	107.5	131.5	85.9	82.8	81.7
33.25	76.8	50.7	22.0	19.3	10.8

A comparison of the obtained values shows that in the models with the GSI value of 50, the blast damage expands by 33 m. The expansion of damage is limited to the distances of 23-33 m, 13-23 m, and 0-13 m, respectively, relative to the blasthole collar, along with the increase in GSI value to 75 and also the increase in D from 0 to 1.

The highest PPV values before and after the discontinuities in the standard models in which the direction of discontinuities is opposite to the slope face showed a reduction of 22-67% for the first discontinuity, 47-75% for the second discontinuity, and 29-68% for the third discontinuity. In models with discontinuities with the same direction of the

slope face, there has been a reduction of 17-75%, 34-57%, and 13-71%, respectively in PPV values.

In general, the greatest values in the first discontinuity belong to the hardest rock mass, and they belong to the weakest rock mass in the third discontinuity. This is the case because, in the hard rock mass, the discontinuities act as the weakest link of a chain while this role is less strong in poor rock mass.

5.5. Statistical study of discontinuities spacing effect

Similar to the previous mode, the highest PPV values on discontinuity surfaces were selected at the distances of 23.25, 28.25, and 33.25 m, and they were presented in Tables 5 and 6. The comparison between similar values in Tables 3 and 4 shows that the PPV value at the blasthole collar decreases along with the increase in the first discontinuity distance. Thus, it contributes to greater damage to the rock mass requiring no fragmentation. However, the PPV value in the second and third discontinuities shows that the decrease in the distance between them exerts some disturbing impacts on the rock mass not requiring its fragmentation. The comparison of similar values in Tables 5 and 6 shows that when the spacing between discontinuities decreases and the discontinuities with the same direction of the slope face, the expansion of blast damage will be greater along with the increase in rock mass strength. This is the case because, according to Figures 6 and 7, the discontinuities lead to an increase in reflections to the surface; however, in the modes where the direction of discontinuities is opposite to the slope face, the waves are reflected into the rock mass.

Table 5. Greatest PPV values above the blasthole collar and discontinuities surface in the first mode of discontinuities and reduced spacing

Location (m) from Blastholes	PPV Max (mm/s)				
	GSI50-D0.7	GSI50-D0	GSI75-D1	GSI75-D0.7	GSI75-D0
0	1004.2	386.3	180.3	169.9	138.5
23.25	316.0	187.7	128.3	77.1	40.6
28.25	174.1	150.2	99.6	67.1	33.2
33.25	164.7	116.5	64.4	44.4	13.1

Table 6. Greatest PPV values above the blasthole collar and discontinuities surface in the second mode of discontinuities and reduced spacing

Location (m) from Blastholes	PPV Max (mm/s)				
	GSI50-D0.7 (1)	GSI50-D0 (1)	GSI75-D1 (1)	GSI75-D0.7 (1)	GSI75-D0 (1)
0	881.1	382.4	193.5	174.8	147.9
23.25	171.0	158.9	148.4	123.0	100.3
28.25	134.0	127.8	91.6	80.5	58.4
33.25	86.5	59.9	30.3	27.4	9.0

5.6. Updating the blast damage factor (D) estimation guide

Hoek et al. in the D estimation guide limited the selection of the appropriate value only to the blasting method [12]. According to the results of this study, the type of rock mass (average or hard), and also the direction and spacing of discontinuities affected the damage expansion and factor D. Thus, the previous estimation guide table was updated as Table 7 to be able to estimate the rock mass damage or the appropriate D more exactly according to the distance from the final wall to the blasting site.

Table 7. Suggested guideline for estimating factor D based on rock mass conditions, direction, and spacing of discontinuities

Rock mass	Average Rock mass				Hard Rock mass			
Conditions	Discontinuities opposite		Discontinuities along		Discontinuities opposite		Discontinuities along	
D Value	A	B	A	B	A	B	A	B
1	-	-	-	-	23-33 m	>33 m	23-33 m	28-33 m
07	>33 m	>33 m	>33 m	>33 m	13-23 m	28-34 m	23-33 m	28-33 m
0	>33 m	>33 m	>33 m	>33 m	>0 m	>0 m	23-33 m	28-33 m

A: Standard model; **B:** reduced discontinuities spacing model

5.7. Analytical analysis

Tables 8 and 9 present the comparison of the greatest PPV values in both modes of effect assessment of the reducing discontinuities spacing relative to the standard models. The rock mass between the discontinuities causes the damping of blasting dynamic pressure. By reducing the spacing, the damping is also reduced and discontinuities play the main role in damping. Thus, as can be seen in the tables, PPV values in these conditions have decreased relative to similar standard conditions.

Table 8. The ratio of effect assessment model PPV of discontinuities spacing to that of standard models with discontinuities in the opposite direction to the slope face

	PPV Max (%)				
Location (m) from Blastholes	**GSI50-D0.7**	**GSI50-D0**	**GSI75-D1**	**GSI75-D0.7**	**GSI75-D0**
23.25	88.9	88.4	94.6	102.9	120.8
28.25	103.9	94.3	125	141.6	137.2
33.25	144.8	127	152.7	209.1	185.2

Table 9. The ratio of effect assessment model PPV of discontinuities spacing to that of standard models with discontinuities with the same direction to the slope face

	PPV Max (%)				
Location (m) from Blastholes	**GSI50-D0.7 (1)**	**GSI50-D0 (1)**	**GSI75-D1 (1)**	**GSI75-D0.7 (1)**	**GSI75-D0 (1)**
23.25	54.3	51.2	75	72.3	70.4
28.25	124.7	97.2	106.7	97.2	71.5
33.25	112.7	118	138	141.7	83.7

6. Conclusions

It is possible to conduct a numerical investigation of the blast damage zone in the rock mass and update the factor D estimation guide table with the dynamic capabilities of the 3D discrete element method based on Hoek's suggestion. Considering these capabilities, the effect of discontinuities on the expansion of the damage zone was examined, and the main results were as follows:

1. In the examination of the probable failure zones, it was determined that the geological discontinuities had a controlling, damping, and reducing role concerning the blast damage. This role of discontinuities became more obvious along with the increase in rock mass strength. Further, fewer qualitative and quantitative failure zones were observed. In the models with discontinuities with the same direction of the slope, the failure zones were controlled to a greater extent, and the toe of the slope was less subject to failure and disturbance.
2. The engineering classification is effective in predicting blast damage due to mentioning rock mass properties. The blast damage is reduced both qualitatively and quantitatively along with the increase in rock mass rating.
3. The empirical models predicting PPV are not able to explain the effect of discontinuities, and the values obtained by these models are not consistent with actual values.
4. A comparison of models with the same GSI and different D showed that parameter D is related to blast damage, and we should use its correct values for the analysis of actual slope stability.
5. The investigation of the highest PPV values before and after the first, second, and third discontinuities (at the distances 13.25, 23.25, and 33.25 m), in the standard models in which the direction of discontinuities is opposite to the slope face, showed an average reduction of 52% in damage per discontinuity. The range of this reduction for each discontinuity is as follows:
   - First discontinuity: 22-67%
   - Second discontinuity: 47-75%
   - Third discontinuity: 29-68%
6. In similar conditions with a discontinuity with the same direction of the slope face, an average reduction of 59% was observed per discontinuity. The range of this reduction for each discontinuity is as follows:
   - First discontinuity: 17-75%
   - Second discontinuity: 34-57%
   - Third discontinuity: 13-71%
7. In all models, the values of D, GSI, and direction of discontinuities are different where the changes in PPV for these differences show the relation between them.
8. When the spacing of discontinuities decreased and the direction of discontinuities was opposite to the slope face, the expansion of blast damage was more limited along with the increase in rock mass strength. If the discontinuities were within an area outside the

blast zone, a more destructive impact is exerted on rock mass along with the decrease in their spacing.

9. The maximum blast damage extends up to 33 m from the blasthole collar. In addition, the expansion of blast damage decreases along with the increase in rock mass strength. A similar study by Haghnejad et al. also showed the expansion of the blast damage to more than 40 m. Based on Hoek`s study, the damages resulting from the blasting can expand as parallel cracks up to 55 meters away into the mine slopes. It can be concluded that the expansion of blast damage depends on the properties of the rock mass and discontinuities, the geometry of the discontinuities, and the quality of the blast.
10. As the distancing of discontinuities decreases, the role of the discontinuities in damping becomes more obvious than that of the rock mass. Furthermore, the discontinuities reduced PPV value by getting further away from blasthole collar, and the next discontinuity created a greater damping relative to the previous one.
11. Numerical modeling capabilities provided the possibility of examining the blasting process and its damages. Thus, according to Hoek's suggestion, we can use it as a useful tool to determine factor D.
12. Based on the conflict between the PPV chart obtained from numerical modeling and the empirical PPV predicting model, it is suggested to use numerical modeling instead of these empirical models to examine the impact of blast damage on large and important slopes.
13. According to Table 8, the damage factor values can be selected as layers parallel to the slope face. In this case, factor D closer to the actual value will be applied to the rock mass, and the use of the H-B failure criterion will also produce more realistic results.
14. Due to the controlling role of discontinuities on damage control, the effect of artificial discontinuities like those developed in the pre-split blasting will be more evident in reducing damage and preventing slope instability.

References

[1]. Yang, J., Lu, W., Jiang, Q., Yao, C., Jiang, S., & Tian, L. (2016). A study on the vibration frequency of blasting excavation in highly stressed rock masses. *Rock Mechanics and Rock Engineering, 49*, 2825-2843.

[2]. Azizabadi, HRM., Mansouri, H., & Fouche, O. (2014). Coupling of two methods, waveform superposition and numerical, to model blast vibration effect on slope stability in jointed rock masses. *Computers and Geotechnics, 61*, 42-49.

[3]. Ainalis, D., Kaufmann, O., Tshibangu, JP., Verlinden, O., & Kouroussis, G. (2016). Modelling the source of blasting for the numerical simulation of blast-induced ground vibrations: A review. *Rock Mechanics and Rock Engineering, 50*, 171-193.

[4]. Rezaei, M. (2023). Monitoring the geotechnical stability of quarry rubble mines of the Kurdistan province. *Iranian journal of engineering geology, 16*(2), 1-18.

[5]. Hoek, E. (2007). Practical rock engineering. *Hock`s Corner*.

[6]. Hoek, E., & Karzulovic, A. (2000). Rock-mass properties for surface mines. *Proceedings Slope Stability in Surface Mining* (Edited by W.A. Hustrulid, M.K. McCarter and D.J.A. Van Zyl (Eds)). Society for Mining, Metallurgy and Exploration, Inc. (SME), Colorado, USA.

[7]. Hoek, E., & Brown, ET. (1980). *Underground excavations in rock*. The Institution of Mining and Metallurgy

[8]. Hoek, E., & Brown, ET. (1988). The Hoek-Brown failure criterion- A 1988 update. *Procedure 15th Canadian Rock Mechanics Symposium*, Toronto.

[9]. Hoek, E., Wood, D., & Shah, S. (1992). A modified Hoek-Brown criterion for jointed rock masses. *Proceedings of the international ISRM symposium on rock characterization*, Chester.

[10]. Eberhardt, E. (2012). The Hoek-Brown failure criterion. *International Journal of Rock Mechanics and Rock Engineering, 45*, 981-988.

[11]. Zuo, J., & Shen, J. (2020). The Hoek-Brown failure criterion- From theory to application. *Springer*.

[12]. Hoek, E., Carranza-Torres, C., & Corkum, B. (2002). Hoek-Brown criterion- 2002 edition. *Procedure NARMS-TAC Conference*, Toronto, 1, 267-273.

[13]. Marinos, P., Marinos, V., & Hoek, E. (2007). Geological strength index (GSI). A characterization tool for assessing engineering properties for rock masses. Lisbon: *Underground works under special conditions Taylor and Francis*.

[14]. Hoek, E., & Brown, ET. (2019). The Hoek-Brown failure criterion and GSI- 2018 edition. *Journal of Rock Mechanics and Geotechnical Engineering, 11*, 445-463.

[15]. Sonmez, H., & Ulusay, R. (1999). Modifications to the Geological Strength Index (GSI) and their applicability to stability of slopes. *International Journal of Rock Mechanics and Mining Sciences, 36*, 743-760.

[16]. Sonmez, H., Gokceoglu, C., & Ulusay, R. (2004). Indirect determination of the modulus of deformation of rock masses based on the GSI system. *International Journal of Rock Mechanics and Mining Sciences, 41*, 849-857.

[17]. Hoek, E., & Diederichs, MS. (2006). Authors' reply to the discussion by H. Sonmez and C. Gokceoglu on their paper ''Empirical Estimation of Rock Mass

Modulus''. *International Journal of Rock Mechanics and Mining Sciences, 43*, 677-678.

[18]. Sonmez, H., & Gokceoglu, C. (2006). Discussion of the paper by E. Hoek and M.S. Diederichs ''Empirical Estimation of Rock Mass Modulus''. *International Journal of Rock Mechanics and Mining Sciences, 43*, 671-676.

[19]. Hoek, E. (2012). Blast damage factor D. *Technical note for Rocscience*.

[20]. Rose, ND., Scholz, M., Burden, J., King, M., Maggs, C., & Havaej, M. (2018). Quantifying transitional rock mass disturbance in open pit slopes related to mining excavation. *Slope stability XIV International Congress on Energy and Mineral Resources*, Seville, Spain.

[21]. Lu, WB., Hu, YG., Yang, JH., Chen, M., & Yan, P. (2013). Spatial distribution of excavation induced damage zone of high rock slope. *International Journal of Rock Mechanics and Mining Sciences, 64*,181-191.

[22]. Sheng, S., Qian, Z., Brackley, W., & Li, AJ. (2014). Rock mass disturbance effects on slope assessments using limit equilibrium method. *23rd Australasian conference on the mechanics of structures and materials (ACMSM23)*, Australia.

[23]. Qian, ZG., Li, AJ., Lyamin, AV., & Wang, CC. (2017). Parametric studies of disturbed rock slope stability based on finite element limit analysis methods. *Computers and Geotechnics, 81*,155-166.

[24]. Haghnejad, A., Ahangari, K., Moarefvand, P., & Goshtasbi, K. (2018). Numerical investigation of the impact of geological discontinuities on the propagation of ground vibrations. *Geomechanics and Engineering 14*(6), 545-552.

[25]. Haghnejad, A., Ahangari, K., Moarefvand, P., & Goshtasbi, K. (2019). Numerical investigation of the impact of rock mass properties on propagation of ground vibration. *Natural Hazards, 96*, 587-606.

[26]. Chamanzad, M.A., & Nikkhah, M. (2020). Sensitivity Analysis of Stress and Cracking in Rock Mass Blasting using Numerical Modelling. *Journal of Mining and Environment, 11*(4), 1141-1155.

[27]. Afrasiabian, B., Ahangari, K., & Noorzad, A. (2020). Study on the effects of blast damage factor and blast design parameters on the ground vibration using 3D discrete element method. *Innovative Infrastructure Solutions, 5*(2), 1-4.

[28]. Afrasiabian, B., Ahangari, K., & Noorzad, A. (2021). Study on the effect of air deck on ground vibration and development of blast damage zone using 3D discrete element numerical method. *Arabian Journal of Geosciences, 14*(1267).

[29]. Kaveh-Ahangaran, D., Ahangari, K., & Eftekhari, M. (2022). Numerical analysis of blast-induced damage in rock slopes. *Innovative Infrastructure Solutions, 7*, 1-18.

[30]. Mousavi, SA., Ahangari, K., & Goshtasbi, K. (2022). An Investigation into Bench Health Monitoring under Blast Loading in Hoek-Brown Failure Criterion using the Finite Difference Method. *Journal of Mining and Environment, 13*(3), 875-889.

[31]. Mousavi, SA., Ahangari, K., & Goshtasbi, K. (2023). Impact of the Layering of Blast-Induced Damage Factors in the Hoek–Brown Failure Criterion on the Bench Damage Monitoring of Mines. *Rudarsko-geološko-naftni zbornik, 38*(1), 93-104.

[32]. Wyllie, DC., & Mah, C. (2004). Rock slope engineering- Civil and mining. *Taylor & Francis*, New York, USA.

[33]. Hustrulid, W. (1999). Blasting principles for open pit mining- General design concept. *Balkema*, Rotterdam.

[34]. Rezaei, M., & Seyed-Mousavi, S.Z. (2024). Slope stability analysis of an open pit mine with considering the weathering agent: Field, laboratory and numerical studies. *Engineering Geology, 333*(107503).

[35]. Hoek, E., & Brown, ET. (1997). Practical estimates of rock mass strength. *International journal of rock mechanics and mining sciences, 34*(8), 1165-1186.

[36]. Rocscience RocLab. (2007). *Tutorial Manual*.

[37]. Yilmaz, O., & Unlu, T. (2013). Three dimensional numerical rock damage analysis under blasting load. *Tunnelling and Underground Space Technology, 38*, 266-278.

[38]. Babanouri, N., Mansouri, H., Karimi-Nasabm, S., & Bahaadini, M. (2013). A coupled method to study blast wave propagation in fractured rock masses and estimate unknown properties. *Computers and Geotechnics, 49*, 134-142.

[39]. Wei-Hua, W., Xi-Bing, L., Yu-Jun, Z., Zi-Long, Z., & Yi-Ping. Z. (2006). 3DEC modeling on effect of joints and interlayer on wave propagation. *Transactions of Nonferrous Metals Society of China, 16*, 728-734.

[40]. Mckenzie, CK. (1993). Methods of improving blasting operations. Hudson, I.A., Editor. Comprehensive rock engineering: excavation, support and monitoring, Vol. 4, *Pergamon Press*, Oxford.

[41]. Jong, Y., Lee, C., Jeon, S., Cho, Y., & Shim, D. (2005). Numerical modeling of the circular-cut using particle flaw code. *31st Annular Conference of Explosives and Blasting Technique*, Orlando, USA.

[42]. Aliabadian, Z., & Sharafisafa, M. (2014). Numerical modeling of presplitting controlled method in continuum rock masses. *Arabian Journal of Geosciences, 7*, 5005-5020.

[43]. Mortazavi, A., & Katsabanis, PD. (2001). Modelling burden size and strata dip effects on the surface blasting process. *International Journal of Rock*

Mechanics and Mining Sciences, 38, 481-498.

[44]. Resende, JRP. (2010). An investigation of stress wave propagation through rock joints and rock masses. *Ph.D. Thesis, Universidade do Porto*, Portugal.

[45]. Drukovanyi, MF., Kravtsov, VS., Chernyavskii, YE., Reva, VV., & Zerkov, SN. (1976). Calculation of fracture zones created by exploding cylindrical charges in ledge rocks. *Soviet Mining Science, 12*(3), 292-295.

[46]. Liu, Q. (2002). Estimation of dynamic pressure around of fully loaded basthole in rock. *Fragblast, 7*, 267-272.

[47]. Hustrulid, W., Bennett, R., Ashland, F., & Lenjani, M. (1992). A new method for predicting the extent of blast damage zone. *Proc Blasting Conference paper No 3*, Gyttorp: Nitro Nobel.

[48]. Persson, PA., Holmberg, R., & Lee, J. (1993). Rock blasting and explosive engineering. *CRC Press*, London, United Kindom.

[49]. Bhandari, S. (1997). Engineering rock blasting operations. *Rotterdam, Balkema*.

[50]. Itasca Consulting Group Inc. (2018). 3DEC 5.2 User's guide. *Minneapolis*, USA.

[51]. Haghnejad, A., Ahangari, K., & Noorzad, A. (2014). Investigation on various relations between uniaxial compressive strength, elasticity and deformation modulus of Asmari formation in Iran. *Arabian Journal for Science and Engineering, 39*, 2677-2682.

[52]. Kumar, R., Choudhury, D., & Bhargava, K. (2016). Determination of blast-induced ground vibration equations for rocks using mechanical and geological properties. *Journal of Rock Mechanics and Geotechnical Engineering, 8*(3), 341-349.

بررسی تاثیر ناپیوستگی‌ها بر پارامتر آسیب انفجار در معیار شکست هوک-براون برای شیب سنگی با استفاده از مدلسازی المان مجزای سه‌بعدی

داریوش کاوه آهنگران[1]، کاوه آهنگری[1*] و مصلح افتخاری۲

۱- گروه مهندسی معدن، دانشگاه آزاد اسلامی، واحد علوم و تحقیقات، تهران، ایران
۲- گروه مهندسی معدن، دانشگاه تربیت مدرس، تهران، ایران

ارسال ۲۰۲۴/۰۵/۱۵، پذیرش ۲۰۲۴/۰۹/۱۷

* نویسنده مسئول مکاتبات: Kaveh.ahangari@gmail.com

چکیده:

آسیب انفجار بر روی پایداری شیب‌ها نقش مهمی در سودآوری و ایمنی معادن دارد. تعیین این آسیب نیز در معیار شکست هوک-براون به طور گسترده مورد استفاده قرار می گیرد. البته این آسیب به‌عنوان یک عامل تعدیل‌کننده در این معیار شکست استفاده می‌شود و تعیین دقیق آن چالشی مهم در مهندسی سنگ تلقی می شود. این مطالعه با هدف بررسی تأثیر ساختارهای زمین‌شناسی در ضریب آسیب انفجار با استفاده از مدل‌سازی المان‌های مجزای سه‌بعدی دو شیب با جهات مختلف ناپیوستگی‌های زمین‌شناسی انجام شد. فشار دینامیکی انفجار نیز در سه چال انفجاری شبیه‌سازی شده است. برای اطمینان از نتایج مدل‌سازی، سایر ویژگی‌های دینامیکی مدل بر اساس مطالعات تاییدشده انتخاب شده‌اند. تجزیه و تحلیل تحلیلی بر اساس مناطق شکست (ناحیه آسیب انفجار) انجام شد و تجزیه و تحلیل‌های کمی و کیفی با استفاده از مقادیر PPV ثبت شده در طول شبیه‌سازی انفجار انجام شد. نتایج نشان می‌دهد که ناپیوستگی‌های زمین‌شناسی، تخریب‌های ناشی از انفجار را کنترل و میرا کرده و کاهش می‌دهند. گسترش آسیب انفجار به‌همراه افزایش مقاومت توده‌سنگ تا ۷۵ درصد کاهش می یابد و آسیب انفجار می‌تواند تا ۳۳ متر همراه با کاهش قدرت گسترش یابد. با کاهش فاصله ناپیوستگی‌ها، نقش ناپیوستگی‌ها در میرایی بیشتر از سایر خواص توده‌سنگ می‌شود و ناپیوستگی‌های دورتر از چال انفجار، میرایی بیشتری ایجاد می کند. رابطه بین فاصله از چال انفجاری و مقادیر PPV نشان می دهد که برای دستیابی به نتایج واقعی‌تر تحلیل پایداری شیب، مقادیر ضریب آسیب در معیار شکست هوک-براون باید به‌تدریج و به‌صورت کاهشی در لایه های موازی با سطح شیب اعمال شود.

کلمات کلیدی: ناپیوستگی‌های زمین‌شناسی، اندیس مقاومت زمین‌شناسی، حداکثر سرعت ذرات، پارامتر آسیب انفجار، 3DEC.